International Journal of Non-Linear Mechanics 52 (2013) 73–84

Contents lists available at SciVerse ScienceDirect

International Journal of Non-Linear Mechanics

journal homepage: www.elsevier.com/locate/nlm

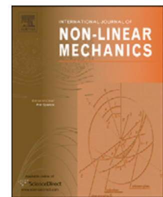

Influence of size effect and elastic boundary condition on the pull-in instability of nano-scale cantilever beams immersed in liquid electrolytes

Aminreza Noghrehabadi *, Mohsen Eslami, Mohammad Ghalambaz

Department of Mechanical Engineering, Shahid Chamran University of Ahvaz, Ahvaz, Iran

ARTICLE INFO

Article history:
Received 7 August 2012
Received in revised form
13 January 2013
Accepted 13 January 2013
Available online 31 January 2013

Keywords:
Liquid electrolytes
Size effect
Electrochemical force
van der Waals
Pull-in instability
Adomian decomposition

ABSTRACT

In this study, the static pull-in instability of nanocantilever beams immersed in a liquid electrolyte is theoretically investigated. In modeling the nanocantilever beam, the effects of van der Waals forces, elastic boundary condition and size dependency are considered. The modified couple stress theory, containing material length scale parameter, is used to interpret the size effect which appears in micro/nanoscale structures. The modified Adomian decomposition (MAD) method is used to gain an approximate analytical expression for the critical pull-in parameters which are essential for the design of micro/nanoactuators. The results show that the beam can deflect upward or downward, based on the values of the non-dimensional parameters. It is found that the size effect greatly influences the beam deflection and is more noticeable for small thicknesses. Neglecting size effect overestimates the deflection of the nanobeam. The findings reveal that the increase of ion concentration increases the pull-in voltage but decreases the pull-in deflection. Furthermore, an increase in ion concentration increases the influence of size-dependent effect on pull-in voltage.

© 2013 Elsevier Ltd. All rights reserved.

1. Introduction

A new field of scientific and technological research is introduced due to the development of new materials with the size of a few micro/nanometers such as micro/nano devices. The objective of these devices is to develop faster and better communication systems in addition to smarter and smaller micro/nano devices. Generally, the micro and nanofabrication processes are planar technologies. A typical beam-type micro/nano electromechanical system (MEMS/NEMS) is made of two conductor nanoelectrodes that the upper one is movable and the lower one is fixed. A physical schematic of cantilever nanobeam actuator is depicted in Fig. 1. Applying voltage difference between these two nanoelectrodes causes the movable one deflects downward as a result of electrostatic force. At a critical voltage, pull-in voltage, instability occurs and the movable electrode is pulled-in onto the fixed one. Beam-type MEMS/NEMS is increasingly used in many applications such as accelerometers [1,2], pressure sensors [3], high-quality filters [4], relays [5], nanotweezer [6,7], switches [8] and comb-drive actuators [9].

The first issue that appears at nanoscale is the effect of dispersion forces such as van der Waals attraction. Consider a typical cantilever beam suspended above a surface with a small gap in between. As the gap decreases from micro to nanoscale, several intermolecular forces become important. The intermolecular forces significantly influence the deflection and internal stresses of nanobeam, at nanoscale separations [10,11]. The van der Waals force results from the interaction between instantaneous dipole moments of atoms. This force is significant when separation is less than the retardation length (typically below 20 nm) which corresponds to the transition between the ground and the excited states of the atom [12]. The van der Waals force attraction is proportional to the inverse cube of the separation and is affected by material properties [13]. Capillary force also can be appeared as the result of a volume of liquid trapped underneath the beam during rinsing and drying processes in fabrication. When the beam is placed in a liquid electrolyte, the osmotic (chemical) force appears because of ion concentration difference.

Because of the importance of micro and nanobeams in the recent technologies, many researchers have analyzed and modeled the micro and nanobeams. Generally, there are two main approaches to model the micro and nanoscale beams, namely, the one degree of freedom (1DOF) model and distributed parameter model. The one degree of freedom model considers the beam as a mass and spring which the nonlinear forces act on the mass. In this model, the entire beam has one average displacement. However, most of the significant forces in the range of nanometer are a function of displacement. Furthermore, the method of 1DOF

* Correspondrnce to: Department of Mechanical Engineering, Shahid Chamran University of Ahvaz, PO Box 6135743337, Ahvaz, Iran. Tel: +98 611 3330010 x5678, Mob.: +98916 312 8841; fax: +98 611 3336642.
E-mail addresses: a.r.noghrehabadi@scu.ac.ir, noghrehabadi@scu.ac.ir (A. Noghrehabadi), m-eslami@mscstu.scu.ac.ir (M. Eslami), m.ghalambaz@gmail.com (M. Ghalambaz).

0020-7462/$ - see front matter © 2013 Elsevier Ltd. All rights reserved.
http://dx.doi.org/10.1016/j.ijnonlinmec.2013.01.014

Nomenclature

Symbol physical meaning

A	cross-sectional area of the beam
A_h	Hamaker constant
B	width of beam
c_b	bulk ion concentration
E	young's modulus
e	electronic charge
f_c	chemical (osmatic) per unit beam length
f_e	electrical force per unit beam length
f_{ec}	electrochemical force per unit beam length
f_{vdw}	van der Waals force per unit beam length
g	initial gap between the electrode
I	second moment of cross-sectional area
k_B	Boltzmann constant
K_θ	spring stiffness
L	length of beam
l	length scale parameter
m_{ij}	deviatoric part of couple stress tensor
$q(x)$	external forces
T	absolute temperature
t	thickness of beam
U	strain energy
u	displacement in the x direction
u_0	normalized tip deflection
u_i	components of displacement vector
v	displacement in y direction
w	displacement in z direction
z_c	absolute value of the valence

Greek symbols

α	non-dimensional van der Waals force
β	non-dimensional electrochemical force
δ	size effect parameter
ε	relative permittivity of the dielectric medium between the two electrodes
ε_0	permittivity of vacuum
ε_{ij}	strain tensor
θ_i	components of rotation vector
λ	lame's first constant
λ_{DL}	Debye length
μ	shear modulus
ν	Poisson's ratio
ξ_0	non-dimensional ionic concentration
σ_{ij}	stress tensor
ϕ_2/ϕ_1	non-dimensional voltage ratio
χ_{ij}	symmetric curvature tensor
$\psi(x)$	rotation angle
ψ_1, ψ_2	applied electric potential to two electrodes

fails to obtain the shape of the beam after deflection and the induced resultant stress. It is worth mentioning that the 1DOF methods are simple and, in most cases, an analytical expression for pull-in instability and displacement of the beam can be easily obtained. By contrast, the distributed model considers the beam as a distributed mass each element of which is directly acted by the forces. This model is capable of simulating the shape of the beam after deflection and the induced resultant stress. Osterberg [14] was the first who introduced the one degree of freedom (1DOF) model and obtained an analytical expression for the pull-in parameters about MEMS switches. Considering lumped parameter model (1DOF), some researchers analyzed the electrical force [15–18] and some of them analyzed the simultaneous influence of intermolecular and electrical forces [19–21]. Ou et al. [22] presented a semi-analytical formulation to inspect the behavior of microbeams, subjected to both residual stress gradients and electrostatic loads. Some of the researchers applied distributed parameter model to examine the effect of intermolecular and electrical forces on pull-in parameters of nanobeams [10,23–26]. Because of the nonlinearity of forces in the nanoscale dimensions, the distributed parameter models lead to highly nonlinear differential equations which in most cases is hard to obtain a close form solution. Thus, the power series or numerical methods are needed. As the convergence of numerical methods at the onset of pull-in instability decreases, finding an accurate solution for the pull-in instability of nanobeams using numerical methods becomes more difficult. Hence, in recent researches, the approximate solutions and analytical methods have been utilized to solve the governing differential equations arising from distributed models. Abadyan et al. [27], using MAD theory, considered the influence of van der Waals force and elastic boundary condition (B.C) on the pull-in behavior of NEMS. Noghrehabadi et al. applied power series solution [28] and a monotone method [29] to investigate the deflection and instability of a multi-walled carbon nanotube (MWCNT) under van der Waals attraction. Guo and Zhao [30] investigated the influence of van der Waals and Casimir forces on the instability of electrostatic torsional actuators. Gusso and Delben [31] inspected the effect of Casimir force on the electrostatic torsional actuators made of silicon. It is noticeable that all the above mentioned studies have examined the beams in vacuum.

The second important phenomenon at micro/nanoscale structures is the size dependency of material characteristics. The MEMS/NEMS is very small in size; hence the small scale effects on their behavior are considerable and have significant influence on the accuracy of modeling and designing these elements. Size dependency in micro and nanoscales is experimentally validated. In the micro bending test of thin nickel beams, Stolken and Evans [32] have observed that the plastic work hardening shows a great increase as the beam thickness decreases from 50 to 12.5 μm. Experimental outcomes indicate that the size-dependent behavior is an inherent property of materials when the characteristic size such as thickness or diameter is close to the internal material length scale parameter [32–34].

Recent researches show that the classical continuum mechanics theories are unable to predict and interpret the size-dependent behaviors in micron and sub-micron scale structures [35,36]; hence, new models are needed. Couple stress theory is one of the higher-order continuum theories. This theory contains material length scale parameters, and can explain microstructure related

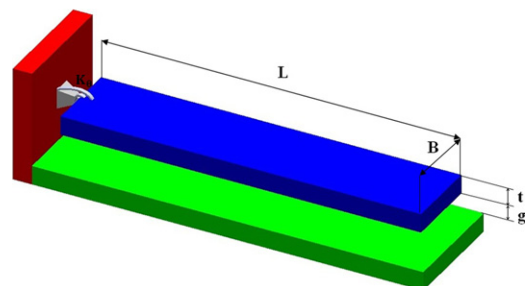

Fig. 1. Scheme of the simply supported nanobeam.

size effects [37]. Yang et al. [38] applied the equilibrium equation of moments of couples and introduced a modified couple stress theory by the classical equilibrium equation of forces and moments of forces in which only one internal length parameter is involved. This new model is successfully employed to estimate the size-dependent effect. Compared to the classical couple stress theory, the modified couple stress theory has two advantages: first, the couple stress tensor is symmetric and second, only one internal length scale parameter is involved.

Based on the total minimum potential energy principle and modified couple stress theory, a new model for an Bernoulli–Euler beam bending is developed by Park and Gao [35]. Kong et al. [39] obtained the governing equation, boundary and initial conditions for a dynamic model of Bernoulli–Euler beams, considering the modified couple stress theory and Hamilton's principle. Rahaeifard et al. [36] used the modified couple stress theory to explain size-dependant behavior of electrostatically actuated microbridge. Zhao et al. [40] modeled a micro clamp–clamp beam by considering fringing field, residual stress and using Analog Equation Method (AEM). They [40] analyzed the influence of size dependency on the static deflection, fundamental frequency and the pull-in parameters. Beni et al. [41] utilized modified couple stress theory to examine the simultaneous influence of van der Waals force and size dependency on NEMS. One of the most considerable materials fulfilling the functions in sensors and switches is silicon. Sadeghian et al. [42] investigated the size-dependent elastic behavior of silicon nano cantilevers and nanowires by experimental measurements.

Characterization of real boundary conditions (B.C.) is the third important effect that must be considered in the simulation of micro/nanoscale structures. The mechanical characteristics of MEMS/NEMS cantilevers totally depend on the choice of material and the boundary support of the elastic structure [43]. Therefore, the boundary support condition requires being theoretically quantified [44] and experimentally validated [45]. Yunqiang et al. [46] studied the effect of boundary conditions on the static and dynamic responses of microplates. The real boundary conditions of structures can be modeled by using artificial springs at the supported end. Rinaldi et al. [47] recommended a method to test MEMS cantilevers under different electro-thermal influences and also presented an experimental approach to quantify the supported boundary condition of atomic force microscopy (AFM) cantilevers.

In many nanotechnology applications such as packaging the nanocomponents before use or in service, the nanocomponents are needed to be placed in liquid electrolytes. In biomedical, a logical application for NEMS devices such as switches, tweezers, and linkages is in body fluids which are typically 0.2 M ionic solutions, mainly NaCL or KCL. There are also ionic liquid applications of NEMS actuators which may include fuel cells, batteries, supercapacitors, filters, electro-osmotic pumps, storage of hydrogen and electroactive polymer actuators. In spite of extensive applications of NEMS actuators in liquid electrolytes only few studies have been carried out to analyze them. Sounart et al. [48] examined MEMS comb-driver electrostatic actuators in sort of liquids which included HeOH, ethylene glycol, isopropyl alcohol. Boyd and Kim [49] applied one degree of freedom (1DOF) model to simulate the electrostatic actuators in liquid electrolytes. Using the solution of linearized Poisson–Boltzman equation, they studied the inherent instability due to van der Waals force and electrochemical forces. Using distributed parameter model, Boyd and Lee [50] investigated a nanocantilever beam in a liquid electrolyte by considering van der Waals, osmotic and electric forces. They examined the effects of bulk ion concentration and surface potential on the tip deflection of the beam.

To the best of authors' knowledge, there is not any investigation to address the influence of size effect and elastic boundary condition on the static deflection and pull-in instability of nanobeams in liquid electrolytes. In the present study, a distributed parameter model based on modified couple stress theory is utilized to simulate the deflection and pull-in instability of nano cantilever beams immersed in liquid electrolytes in the presence of the van der Waals and electrochemical forces. In addition, a rotational artificial spring is used to model the elastic effect of the nanobeam support. The modified Adomian decomposition (MAD) method is employed to solve the constitutive nonlinear differential equation of the nanobeam actuator.

2. Mathematical model

2.1. The modified couple stress theory

In micro and nanoscale structures, the classical continuum mechanics theories are unable to predict and interpret the size-dependent behaviors; hence, new models are needed. The modified couple stress theory has been introduced by Yang et al. [38]. On the basis of this theory, the strain energy (U) in a deformed isotropic linear elastic material occupying region V is a function of both strain and gradient of the rotation vector [39]. Therefore, the strain energy of the nanobeam, shown in Fig.1, can be represented as follow

$$U = \frac{1}{2}\int_V (\sigma_{ij}\varepsilon_{ij} + m_{ij}\chi_{ij})dV \quad (i,j = 1,2,3) \tag{1}$$

where σ_{ij}, ε_{ij}, m_{ij}, χ_{ij} are stress tensor, strain tensor, deviatoric part of couple stress tensor and symmetric curvature tensor, respectively, defined by the following relations

$$\sigma_{ij} = \lambda[tr(\varepsilon_{ij})]I + 2\mu\varepsilon_{ij} \tag{2}$$

$$\varepsilon_{ij} = \tfrac{1}{2}\left[\nabla u_i + (\nabla u_i)^T\right] \tag{3}$$

$$m_{ij} = 2l^2\mu\chi_{ij} \tag{4}$$

$$\chi_{ij} = \tfrac{1}{2}\left[\nabla\theta_i + (\nabla\theta_i)^T\right] \tag{5}$$

where λ and μ are the first and the second Lame's constants. The Lame's constants are material properties that are related to the elastic modulus and Poisson ratio. tr(.) and I are trace function and identity matrix, respectively. l is the material length scale parameter which is small in comparison with the body dimensions. Therefore, its influence might become important as the dimensions of a body diminish to the order of the length scale parameter [51]. Mathematically, the parameter l is the square root of the ratio of the curvature (bending) modulus to shear modulus, and physically is a property measuring the effect of couple stress [35,52]. The material length scale parameter can be determined by experimental methods such as micro/nano indentation test [33,34] and micro bend test [32]. u_i are the components of displacement vector, and θ_i are the components of rotation vector given by

$$\theta_i = \tfrac{1}{2}\mathrm{curl}(u_i) \tag{6}$$

Considering one-dimensional and according to the fundamental hypotheses of Bernoulli–Euler beams, the displacement field can be represented as

$$u = z\psi(x), \quad v = 0, \quad w = w(x) \tag{7}$$

where u, v and w are the x, y and z components of the displacement vector, and $\psi(x)$ is the rotation angle which is related to the

deflection by

$$\psi(x) \approx -\frac{dw(x)}{dx} \tag{8}$$

Considering a small deformation, the non-zero strain components from Eqs. (3), (7) and (8) can be obtained as

$$\varepsilon_{xx} = -z\frac{d^2w(x)}{dx^2}, \quad \text{all other } \varepsilon_{ij} = 0 \tag{9}$$

and from Eqs. (6) and (8)

$$\theta_y = -\frac{dw(x)}{dx}, \quad \theta_x = \theta_z = 0 \tag{10}$$

By substituting Eq. (10) into Eq. (5), the following equations can be derived

$$\chi_{xy} = \chi_{yx} = -\frac{1}{2}\frac{d^2w(x)}{dx^2}, \quad \text{all other } \chi_{ij} = 0 \tag{11}$$

For a slender beam with a large aspect ratio, the Poisson effect can be neglected. Hence, substituting Eq. (9) into Eq. (2) yields

$$\sigma_{xx} = -Ez\frac{d^2w(x)}{dx^2}, \quad \text{all other } \sigma_{ij} = 0 \tag{12}$$

where E is the Young's modulus of the beam. Similarly, substituting Eq. (11) into Eq. (4) gives

$$m_{xy} = -\mu l^2\frac{d^2w(x)}{dx^2}, \quad \text{all other } m_{ij} = 0 \tag{13}$$

where μ is the shear modulus.

2.2. Modeling of the nanobeam

Fig. 1 depicts the physical schematic of a nanoactuator suspended above a ground plane. The actuator is modeled by a simply supported (SS) nanobeam with uniform rectangular cross-section. Here, L is the length, B is the width and t is the thickness of the nanobeam. The initial gap between ground-plane and nanobeam is g. The nanobeam is immersed in a liquid electrolyte.

It is assumed that the beam is homogeneous and linear elastic. In order to model the real boundary condition for the SS beam, an artificial angular spring with a spring stiffness of K_θ is used. Considering the static deflection, substituting Eqs. (9) and (11)–(13) into Eq. (1) and adding the elastic energy of the spring, the energy of the system can be obtained as

$$U = \frac{1}{2}\int_0^L \int_A Ez^2\left(\frac{d^2w}{dx^2}\right)^2 dAdx + \frac{1}{2}\int_0^L \int_A \mu l^2\left(\frac{d^2w}{dx^2}\right)^2 dAdx + \frac{1}{2}K_\theta\left(\frac{dw(0)}{dx}\right)^2 \tag{14}$$

Simplifying Eq. (14) yields

$$U = \frac{1}{2}\int_0^L \left(EI + \mu Al^2\right)\left(\frac{d^2w}{dx^2}\right)^2 dx + \frac{1}{2}K_\theta\left(\frac{dw(0)}{dx}\right)^2 \tag{15}$$

where A is cross-sectional area of the beam. I is the second moment of cross-sectional area as

$$I = \int_A z^2 dA \tag{16}$$

The work done by the external forces, $q(x)$, can be written as

$$V = \int_0^L q(x)w(x)dx \tag{17}$$

According to the minimum total potential energy principle, the governing equilibrium equation is given by

$$\delta\,\Pi = \delta(U - V) = 0 \tag{18}$$

where δ denotes the variation symbol.

Substituting Eqs. (15) and (17) into Eq. (18) leads to

$$\delta\left\{\int_0^L \left(\frac{1}{2}\left(EI + \mu Al^2\right)\left(\frac{d^2w}{dx^2}\right)^2 - qw\right)dx + \frac{1}{2}K_\theta\left(\frac{dw(0)}{dx}\right)^2\right\}$$
$$= \int_0^L \left(\left(EI + \mu Al^2\right)\left(\frac{d^2w}{dx^2}\right)\delta w'' - q\delta w\right)dx + K_\theta\left(\frac{dw(0)}{dx}\right)\delta w' = 0 \tag{19}$$

Integration by parts yields

$$\int_0^L \left(\left(EI + \mu Al^2\right)\tfrac{d^4w}{dx^4} - q(x)\right)\delta w dx + K_\theta\tfrac{dw(0)}{dx}\delta w'(0)$$
$$+\left(EI + \mu Al^2\right)\frac{d^2w}{dx^2}\delta w'\Big|_0^L - \left(EI + \mu Al^2\right)\frac{d^3w}{dx^3}\delta w\Big|_0^L = 0 \tag{20}$$

Thus, the governing equilibrium equation of micro/nanobeam is derived as

$$\left(EI + \mu Al^2\right)\frac{d^4w}{dx^4} = q(x) \tag{21}$$

It is obvious that by substituting $l=0$ in Eq. (21), the modified couple stress theory is reduced to the classical theory. The boundary conditions of a simply supported beam are

$$w(0) = \frac{d^3w(L)}{dx^3} = \frac{d^2w(L)}{dx^2} = 0 \tag{22}$$

$$\left(EI + \mu Al^2\right)\frac{d^2w(0)}{dx^2} = K_\theta\frac{dw(0)}{dx} \tag{23}$$

In most cases of micro/nanobeams $L > 10$ g, and as a result the effect of finite kinematics (large deformations) has been neglected [53–56], therefore, this effect is not considered in the present work. Moreover, the damping effect is not taken into account in the case of mechanical equilibrium [57]. In liquid electrolytes, the net force per unit length of the beam due to double layer interaction is sum of the chemical (osmotic) force per unit beam length (f_c) and electrical force per unit beam length (f_e). As the nanobeam is completely immersed in the liquid electrolyte, the capillary force can be neglected. Hence, the external forces along the beam are sum of the van der Waals force per unit length (f_{vdw}) and electrochemical force per unit length (f_{ec})

$$q(x) = f_{vdw} + f_{ec} \tag{24}$$

Using the Lifshitz theory, the van der Waals force per unit length of the beam can be calculated as [13]

$$f_{vdw} = -\frac{A_hB}{6\pi(g+w)^3} \tag{25}$$

where A_h is Hamaker constant (normally $A_h = 0.4\text{–}4 \times 10^{-20}$ J). The difference between the osmotic pressure of the interstitial solution and the bulk solution gives the osmotic pressure (repulsive pressure) [58]

$$\Pi = k_BT\sum_i (c_i^{\pm} - c_i^{bulk}) \tag{26}$$

where $k_B = 1.38054 \times 10^{-23}$ J K^{-1} is the Boltzmann constant, T is the absolute temperature, c^{bulk} is bulk concentration and $c^{\pm}$ is the concentration of positive and negative ions for a dilute electrolytic solution which is represented by the Boltzmann law as follow [58]

$$c^{\pm} = c_b\exp(\mp z_ce\psi/k_BT) \tag{27}$$

In the above relation, c_b is the bulk ion concentration and assumed to be equal for both ions, z_c is the absolute value of the valence, $e = 1.602 \times 10^{-19}$ C is the electronic charge and ψ is the electrical potential. By using Eqs. (26) and (27) and supposing the bulk electric potential is zero, the chemical (osmotic) force per

unit length is determined as

$$f_c = \Pi\, B = 2Bk_BTc_b\cosh\left(\frac{z_ce\psi}{k_BT}\right) - 2Bk_BTc_b = 2k_BTc_bB\left(\cosh\left(\frac{z_ce\psi}{k_BT}\right) - 1\right) \tag{28}$$

For small values of electric potential, the chemical force can be approximated by Taylor's series

$$f_c = 2k_BTc_bB\left(\frac{z_ce\psi}{k_BT}\right)^2 \tag{29}$$

For parallel plates the capacitance is denoted by

$$C = \frac{\varepsilon\varepsilon_0 A}{g} \tag{30}$$

where ε is relative permittivity of the dielectric medium between two electrodes and $\varepsilon_0 = 8.854\times10^{-12}\ \mathrm{C^2\,N^{-1}\,m^{-2}}$ is the permittivity of vacuum. Using Eq. (30) the electrostatic force per unit length for parallel plates can be calculated as

$$f_e = -\frac{1}{2}\frac{\partial C}{\partial g}\psi^2 = -\frac{1}{2}\varepsilon\varepsilon_0 B\left(\frac{\psi}{g}\right)^2 \tag{31}$$

where

$$\frac{\psi}{g} = E = -\nabla\psi \tag{32}$$

E denotes electric filed. Inserting Eqs. (30) and (32) into Eq. (31) the electrostatic force per unit length can be expressed as

$$f_e = -\frac{1}{2}\varepsilon\varepsilon_0 B(\nabla\psi)^2 \tag{33}$$

It is necessary to specify the electric potential (ψ) in determining the chemical and electrostatic forces. The relation between the electric potential and the charge density (ρ) is given by the Poisson equation

$$\nabla^2\psi = -\frac{\rho}{\varepsilon\varepsilon_0} \tag{34}$$

where the charge density is related to concentration of positive(c^+) and negative(c^-) ions

$$\rho = ez_c(c^+ - c^-) \tag{35}$$

Using Eqs. (34), (35) and (27), the Poisson–Boltzmann equation for a symmetric z_c: z_c electrolyte which determines the electric potential is obtained as

$$\nabla^2\psi = -\frac{ez_c(c^+ - c^-)}{\varepsilon\varepsilon_0} = -\frac{z_cec_b}{\varepsilon\varepsilon_0}\left[\exp\left(-\frac{z_ce\psi}{k_BT}\right) - \exp\left(\frac{z_ce\psi}{k_BT}\right)\right] = \frac{2z_cec_b}{\varepsilon\varepsilon_0}\sinh\left(\frac{z_ce\psi}{k_BT}\right) \tag{36}$$

Precise results are attained from Poisson–Boltzmann equation when concentrations are less than 1 M and surface potentials do not transgress 200 mV [13]. Applying the Taylor series expansion with the first term, the Poisson–Boltzmann equation, Eq. (36), can be linearized for small values of electric potential. In this case, the linear Poisson–Boltzmann equation for a dilute electrolytic solution becomes

$$\frac{d^2\psi}{dz^2} = \frac{2z_c^2e^2c_b}{\varepsilon\varepsilon_0 k_BT}\psi = \kappa^2\psi \tag{37}$$

which is the Debye–Hückel approximation and proceeding from the assumptions that the deflections are small, the central ion is a point charge and each ion is surrounded by ions of opposite charge. In the above equation, $\kappa^2 = 2z_c^2e^2c_b/\varepsilon\varepsilon_0k_BT$, and $1/\kappa$ is the Debye length. Eq. (37) has a solution in the form of

$$\psi = D_1\cosh\kappa z + D_2\sinh\kappa z \tag{38}$$

where constants D_1 and D_2 can be determined by solving the resulting algebraic equations for the general case of two parallel plates with the boundary conditions ψ $(z=0) = \psi_1$ and ψ $(z=g+w) = \psi_2$. Therefore, Eq. (38) is written as

$$\psi = \psi_1\cosh(\kappa z) + \frac{\psi_2 - \psi_1\cosh(\kappa(g+w))}{\sinh(\kappa(g+w))}\sinh(\kappa z) \tag{39}$$

From Eqs. (29), (33) and (39), the electrochemical force can be calculated as

$$f_{ec} = f_e + f_c = B\varepsilon\,\varepsilon_0\kappa^2\frac{\psi_1^2}{\sinh^2(\kappa(w+g))}\left\{\frac{\psi_2}{\psi_1}\cosh(\kappa(w+g)) - \frac{1}{2}\left[1 + \left(\frac{\psi_2}{\psi_1}\right)^2\right]\right\} \tag{40}$$

where ψ_1 and ψ_2 are the applied electric potential between ground plane and cantilever beam. Neglecting the effect of the electrolyte on the van der Waals force and substituting Eqs. (24), (25) and (40) into (21), the governing nonlinear differential equation of the nanobeam is obtained as

$$\left(EI + \mu Al^2\right)\frac{d^4w}{dx^4} = -\frac{A_hB}{6\pi(w+g)^3} + B\varepsilon\varepsilon_0\kappa^2\frac{\psi_1^2}{\sinh^2(\kappa(w+g))}\left\{\frac{\psi_2}{\psi_1}\cosh(\kappa(w+g)) - \frac{1}{2}\left[1 + \left(\frac{\psi_2}{\psi_1}\right)^2\right]\right\} \tag{41}$$

2.3. Non-dimensional formulation:

For convenience, Eq. (41) can be transformed to its non-dimensional form by introducing the following non-dimensional variables,

$$u = \frac{w+g}{g}, \quad X = \frac{x}{L}, \quad \phi = \frac{z_ce\psi}{k_BT} \tag{42}$$

where ϕ corresponds to the value of the applied voltage.

By substituting Eq. (42) into Eq. (41) the non-dimensional governing equation of the nanobeam, which is depicted in Fig. 1, is given by

$$\frac{d^4u}{dX^4} = -\frac{\alpha}{(1+\delta)u^3} + \frac{\beta}{(1+\delta)\sinh^2(\xi_0u)}\left\{\frac{\phi_2}{\phi_1}\cosh(\xi_0u) - \frac{1}{2}\left[1 + \left(\frac{\phi_2}{\phi_1}\right)^2\right]\right\} \tag{43}$$

The five non-dimensional parameters appearing in Eq. (43) are

$$\alpha = B\frac{A_h}{6\pi g^4}\frac{L^4}{EI}, \quad \beta = B\frac{2c_bk_BT\phi_1^2}{g}\frac{L^4}{EI}, \quad \xi_0 = \kappa g, \quad \frac{\phi_2}{\phi_1}, \quad \delta = \frac{\mu Al^2}{EI} \tag{44}$$

where α and β, respectively, denote non-dimensional values of van der Waals force and electrochemical force. ϕ_2/ϕ_1 is the non-dimensional voltage ratio, $\xi_0 = \kappa g$ represents the non-dimensional ionic concentration and δ is non-dimensional size effect ($\delta = 0$ noted the classical theory). Replacing the non-dimensional variables introduced in Eq. (42) into Eqs. (22) and (23), the non-dimensional boundary conditions of a simply supported beam are obtained as

$$u(0) = 1, \quad u''(0) = Ku'(0), \quad u''(1) = u'''(1) = 0 \tag{45}$$

where $K = K_0L/\left(EI + \mu Al^2\right)$.

Using non-dimensional variables, the van der Waals and electrochemical forces can be represented as

$$f_{vdw} = -\frac{\alpha}{u^3} \tag{46}$$

$$f_{ec} = \frac{\beta}{\sinh^2(\xi_0u)}\left\{\frac{\phi_2}{\phi_1}\cosh(\xi_0u) - \frac{1}{2}\left[1 + \left(\frac{\phi_2}{\phi_1}\right)^2\right]\right\} \tag{47}$$

It is noticeable that the model of simply supported beam is reduced to the cantilever beam when the value of spring stiffness tends to infinity. Therefore, it is possible to use the following boundary conditions (B.C.) in the case of cantilever beam

$$u(0)=1,\quad u'(0)=u''(1)=u'''(1)=0 \tag{48}$$

Eq. (43) subject to the boundary conditions, i.e., Eq. (45) or Eq. (48), is the governing differential equation of the nanobeam in the presence of van der Waals and electro mechanical forces. The obtained governing differential equation, Eq. (43), is fourth order and highly nonlinear. Hence, deriving a close form exact solution is not easy. In order to solve this equation subject to each of the boundary conditions, i.e., Eq. (45) or Eq. (48), the modified Adomian decomposition method is utilized.

3. Analytical solution

Modified Adomian decomposition method is employed to solve the nonlinear constitutive governing equation of the nanobeam, Eq. (43). The Adomian polynomials are very powerful to solve non-linear differential equations [59–61]. Different modifications of Adomian decomposition method have been proposed by recent researchers [62–66]. Here, the modified Adomian decomposition method proposed by Wazwaz [59] is utilized to analysis the pull-in behavior of cantilever NEMS.

Applying MAD method, the deflection of the nanobeam in Eq. (43) can be written as follows

$$u(X)=\sum_{n=0}^{\infty}u_n(X) \tag{49}$$

$$\sum_{n=0}^{\infty}u_n(X)=C_0+C_1X+\frac{1}{2!}C_2X^2+\frac{1}{3!}C_3X^3 -\frac{1}{(1+\delta)}L^{-4}\left[\alpha\sum_{n=0}^{\infty}D_n(X)-\beta\frac{\phi_2}{\phi_1}\sum_{n=0}^{\infty}E_n(X)+\beta\left[\frac{1}{2}\left(1+\left(\frac{\phi_2}{\phi_1}\right)^2\right)\right]\sum_{n=0}^{\infty}F_n(X)\right] \tag{50}$$

In above equation the functions D_n, E_n and F_n are defined as

$$D_n=\frac{1}{u^3},\quad E_n=\frac{\cosh(\xi_0 u)}{(\sinh(\xi_0 u))^2},\quad F_n=\frac{1}{(\sinh(\xi_0 u))^2} \tag{51}$$

Thus, by using MAD method, the deflection of the nanobeam in Eq. (43) is obtained (see the Appendix)

$$u(X)=C_0+C_1X+\frac{1}{2!}C_2X^2+\frac{1}{3!}C_3X^3-\frac{1}{4!}\frac{1}{(1+\delta)}X^4\left(\alpha-\beta\frac{\phi_2}{\phi_1}\frac{\cosh(\xi_0)}{\sinh(\xi_0)^2}+\beta\left(1+\left(\frac{\phi_2}{\phi_1}\right)^2\right)\frac{1}{2\sinh(\xi_0)^2}\right) + \frac{1}{(1+\delta)}\left(3\alpha+\beta\frac{\phi_2}{\phi_1}\frac{\xi_0}{\sinh(\xi_0)}\left(1-\frac{2\cosh(\xi_0)^2}{\sinh(\xi_0)^2}\right)+\beta\left(1+\left(\frac{\phi_2}{\phi_1}\right)^2\right)\frac{\xi_0\cosh(\xi_0)}{\sinh(\xi_0)^3}\right) \times\left(\frac{C_1}{5!}X^5+\frac{C_2}{6!}X^6+\frac{C_3}{7!}X^7+\frac{1}{8!}\frac{1}{(1+\delta)}X^8\left(-\alpha+\beta\frac{\phi_2}{\phi_1}\frac{\cosh(\xi_0)}{\sinh(\xi_0)^2}-\beta\left(1+\left(\frac{\phi_2}{\phi_1}\right)^2\right)\frac{1}{2\sinh(\xi_0)^2}\right)\right)+\cdots \tag{52}$$

The constants C_0, C_1, C_2 and C_3 are determined by solving the resultant algebraic equation from boundary conditions, i.e., Eq. (45). In order to verify the accuracy of the obtained results, the governing differential equation of nanobeam, i.e., Eq. (43), is numerically solved using MAPLE commercial software. Table 1 shows the difference between the numerical solution and the MAD method for normalized tip deflection (u_0) of simply supported (SS) and cantilever (C) beams types. The normalized tip deflection is defined as

$$u_0=\frac{u(X)}{g}\Big|_{X=1} \tag{53}$$

As seen, evaluating more terms of the series solution results in a higher accuracy. The eight terms of modified Adomian solution show sufficient accuracy for the engineering applications. Therefore, in the following section, the calculations are performed using eight terms of Adomian series for convenience.

Before solving Eq. (43), at first the MAD method is tested against the published solutions by Boyd and Lee [50] for the bending of a cantilever beam in liquid electrolytes which is based on the classical theory. Neglecting the size effect, i.e., $\delta=0$, and assuming a cantilever beam, i.e., $K\to\infty$, the present work reduces to the work of Boyd and Lee [50]. Fig. 2 shows the influences of the applied voltage, β, on the normalized tip deflection, u_0, of the cantilever beam for $\alpha=0$, $\phi_2/\phi_1=0.1$ and $\xi_0=1$. It can be observed that the normalized tip deflection would increase with an increase in the input voltage. The critical value of $\beta_{PI}=5.24$ occurs at $u_{PI}=-0.386$ which is in very good agreement with the finite element solution reported by Boyd and Lee [50]. It is worth noticing that u_{PI} corresponds to tip deflection of the beam (the maximum deflection of the beam) at the onset of instability.

In next section a simply supported beam, a cantilever beam and a case study of a microactuator will be considered, respectively, to investigate the pull-in behavior of beam-type MEMS/NEMS.

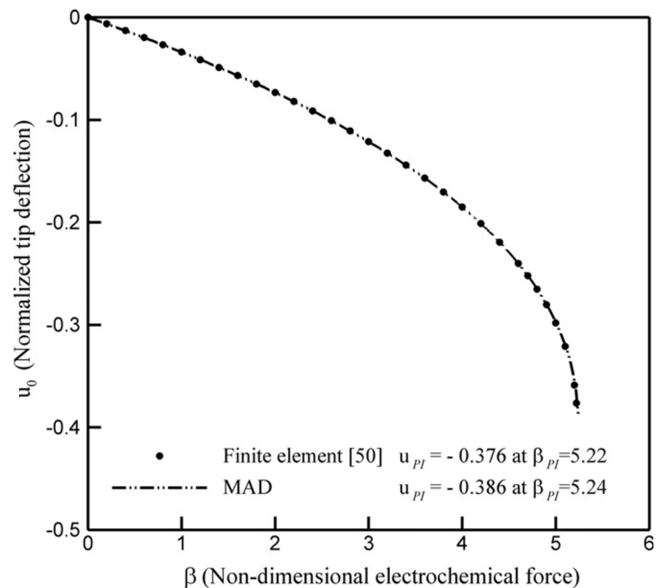

Fig. 2. β versus u_0 when $\alpha=0$, $\phi_2/\phi_1=0.1$ and $\xi_0=1$.

Table 1
Comparison between MAD and numerical solution in typical NEMS deflection.

Case	MAD				Numerical
	Five terms (X^{16})	Six terms (X^{20})	Seven terms (X^{24})	Eight terms (X^{28})	
SS beam ($\alpha=\beta=\zeta=1$, $\phi_2/\phi_1=0.1$, $K=30$, $\delta=0.5$)	−0.16763	−0.16983	−0.16996	−0.17003	−0.17004
Error %	1.417	0.123	0.047	0.006	–
C beam ($\alpha=\beta=\zeta=1$, $\phi_2/\phi_1=0.1$, $\delta=0.5$)	−0.13916	−0.14008	−0.14012	−0.14013	−0.14014
Error %	0.699	0.043	0.014	0.007	–

4. Results and discussion

4.1. Simply supported beam (SS beam)

In order to investigate the effect of elastic B.C. on the pull-in instability of simply supported (SS) nanobeams, the governing equation i.e. Eq. (43) subject to boundary conditions of Eq. (45) is solved. Fig. 3 illustrates the influence of spring stiffness (K) on the deflection of SS beam. By increasing stiffness the flexibility of the supported end is decreased, and consequently, there is less deflection toward the substrate. As the spring stiffness increases, the pull-in instability voltage increases. This figure clearly depicts that as the stiffness of supported end is increased, more voltage is needed to achieve a special deflection. Fig. 4 shows the relationship between electrochemical force (β) and normalized tip deflection for various values of K. It is seen from this figure that an increase in spring stiffness would increase the pull-in voltage. Increasing spring stiffness leads to a decrease in flexibility of the supported end, and hence, it causes the decreasing of the normalized tip deflection and increasing of pull-in voltage. Figs. 3 and 4 depict that the instability of NEMS intensely depends on the sort of applied boundary condition.

4.2. Cantilever beam

In this section the governing differential equation of the nanobeam, i.e., Eq. (43), subject to the boundary conditions of Eq. (48) is solved in order to investigate the pull-in behavior of nanocantilever beam-type. Fig. 5 depicts the variation of normalized tip deflection as a function of ϕ_2/ϕ_1 for selected values of the size effect parameter. This figure reveals that increasing size effect increases the critical ratio ϕ_2/ϕ_1 and normalized tip deflection at the onset of pull-in instability. Therefore, it is possible to use a beam with high size effect parameter in applications in which a large magnitude of tip deflection is required before appearing of the pull-in instability. As can be seen in Fig. 5, for $\phi_2/\phi_1=0.52$ and $\phi_2/\phi_1=7.006$ the value of cantilever tip deflection reaches zero. In these two points the van der Waals and electrochemical forces are equal, but they are in opposite direction. For $0.52<\phi_2/\phi_1<7.006$, the total force at the tip is repulsive which causes the beam gets far from the substrate. As shown, the curve of $\delta=0$ intersects the curves of $\delta>0$ at least at two points. The maximum normalized tip deflections for different values of size effect are the places in which the van der Waals force has its minimum value and the electrochemical force is in maximum repulsive value. The places of maximum tip deflection can be of interest to design micro/nanoactuators.

Fig. 6 demonstrates the influence of size effect parameter on electrochemical force (β) and normalized tip deflection at the pull-in point. This figure interestingly reveals that increasing the value of size effect parameter would increase pull-in voltage, but it does not have significant effect on the normalized tip deflection at the onset of instability (pull-in deflection). Therefore, a nanobeam with higher size effect parameter can be used to have a specific movement in a higher voltage.

Fig. 7 shows the effect of van der Waals force on the normalized tip deflection of the cantilever beam. Because of intermolecular force the beam deflects, even without implying voltage. As seen, augmentation of the van der Waals force decreases the pull in voltage and

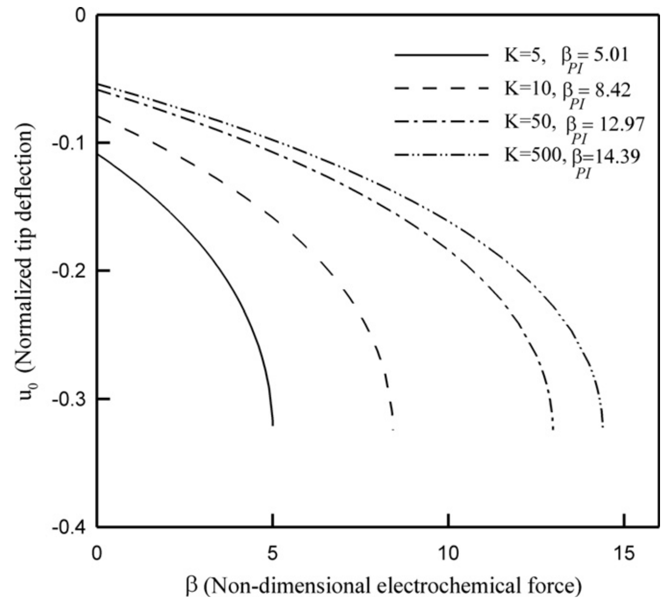

Fig. 4. Effects of spring stiffness on cantilever tip deflection and β for $\alpha=0.5$, $\delta=0.3$, $\phi_2/\phi_1=0.1$, $\xi_0=1.5$.

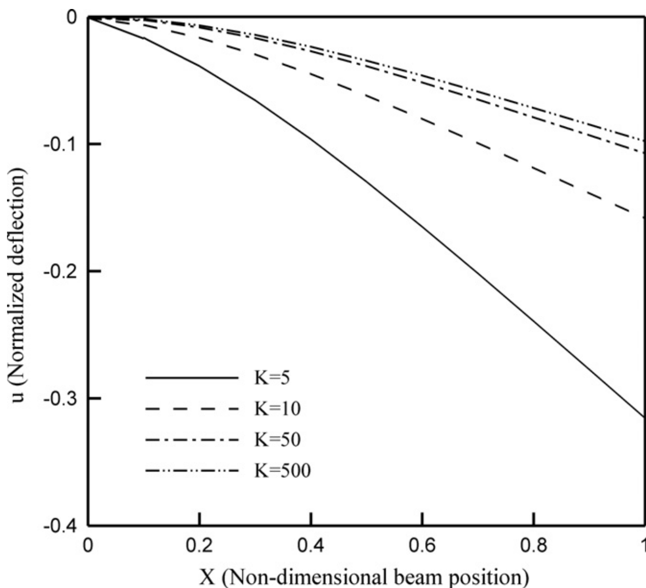

Fig. 3. Deflections of the SS beam for different values of K when $\alpha=0.5$, $\beta=5$, $\delta=0.3$, $\phi_2/\phi_1=0.1$, $\xi_0=1.5$.

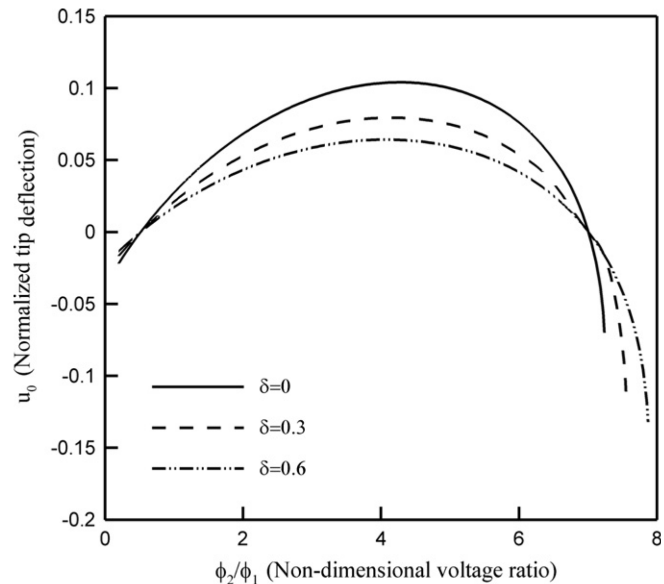

Fig. 5. Effects of size dependency on normalized tip deflection and critical ratio ϕ_2/ϕ_1 for $\xi_0=\beta=2$, $\alpha=0.2$.

pull-in deflection (normalized tip deflection at the onset of instability). As the van der Waals force is a function of the inverse cube of separation, it is concluded that in order to have a nanobeam which operates in high voltages, the distance between two electrodes should be increased (in this state the van der Waals force is reduced).

Fig. 8 shows the influence of the size effect parameter on the van der Waals attraction and cantilever tip deflection in the absence of electrochemical force. This figure indicates that the critical value of non-dimensional van der Waals force (α_c) is dependent on the size effect parameter and increases as the size effect parameter increases. The critical values of α for various values of the size effect parameter are shown in Table 2.

The detachment length is the maximum length (L_{max}) of the electrode actuators that does not adhere to the substrate due to the van der Waals force. When the gap between the electrode and substrate is adequately small, the electrode might adhere to the substrate due to the van der Waals force. In this case, if the length of the actuators is known, the minimum gap (g_{min}) between the two electrodes can be calculated. The detachment length and minimum gap are fundamental design parameters for MEMS and NEMS actuators and are obtained by substituting the value of α_c into Eq. (44) [55]. Based on the results of Table 2 and for $\delta=0$, the L_{max} and g_{min} are

$$L_{\max}=g\sqrt[4]{\frac{0.602\pi Et^3}{A_h}},\quad g_{\min}=L\sqrt[4]{\frac{A_h}{0.602\pi Et^3}}\text{(Numerical method)} \tag{54}$$

$$L_{\max}=g\sqrt[4]{\frac{0.6045\pi Et^3}{A_h}},\quad g_{\min}=L\sqrt[4]{\frac{A_h}{0.6045\pi Et^3}}\text{ (MAD method)} \tag{55}$$

Fig. 8 and Eqs. (54) and (55) reveal that the modified couple stress theory ($\delta\neq 0$) predicts larger L_{max} and smaller g_{min} than classical theory ($\delta=0$).

4.3. Case study with microactuators

In order to study the pull-in instability of microactuators, Eq. (43) subject to boundary conditions of Eq. (48) is solved for a silicon micro cantilever beam actuator. This cantilever is considered as a case study that the geometric data and constitutive material of the beam are identified in Table 3. The applied potential to the electrodes has the same magnitude but opposite sign, $\psi_2=-\psi_1$.

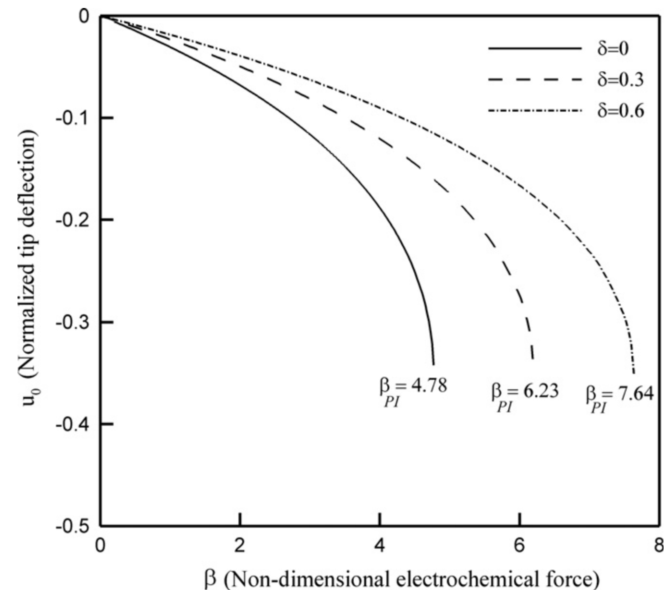

Fig. 6. Effects of size dependency on pull-in parameters for $\alpha=0$, $\phi_2/\phi_1=0.5$, $\xi_0=0.5$.

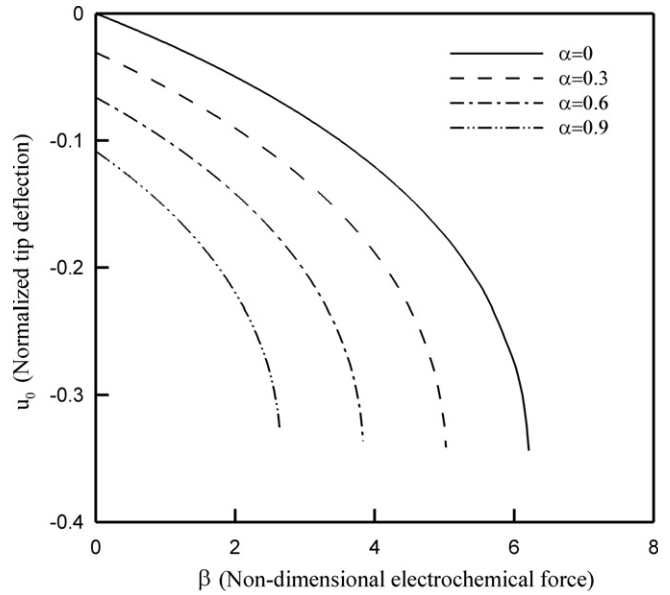

Fig. 7. Effects of van de Waals force on cantilever tip deflection and β for $\delta=0.3$, $\phi_2/\phi_1=0.5$, $\xi_0=0.5$.

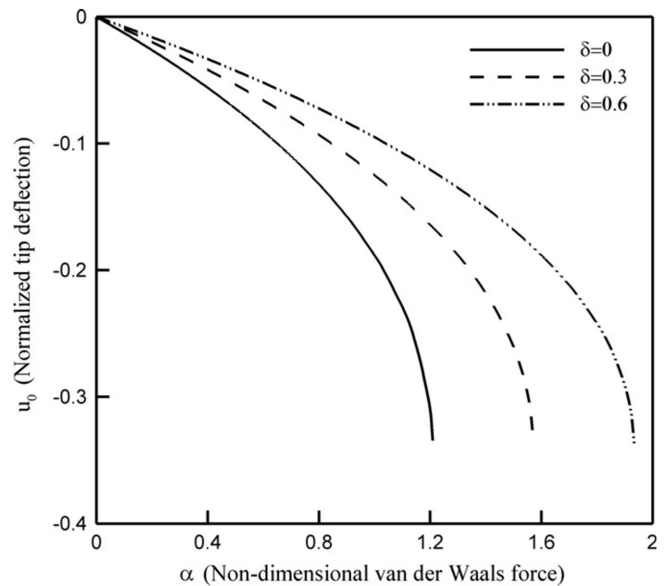

Fig. 8. Effect of size dependency on α and cantilever tip deflection when $\beta=0$.

Table 2
Critical values of α_c versus size effect parameters.

Method	α_c		
	$\delta=0$	$\delta=0.3$	$\delta=0.6$
Numerical	1.204	1.566	1.927
MAD	1.209	1.571	1.934

Fig. 9 depicts the effect of beam thickness on displacement and also makes a comparison between modified couple stress (with size effect) and classical (without size effect) theories. This figure obviously reveals that the size effect greatly influences the beam deflection and is more noticeable for small thicknesses. It is shown that the decrease of beam thickness leads to high

Table 3
Material and geometrical parameters of silicon microactuator. Rahaeifard [56].

Parameter		Value
L	Length of beam	$75-250$ (μm)
t	Thickness of beam	Input value
g	Distance from the base	Input value
E	Young's modulus	169.2 (GPa)
μ	Shear modulus	65.8 (GPa)
A_h	Hamaker constant	0.4×10^{-20} (J)
l	Length scale parameter	0.592 (μm)
T	Temperature	298 (K)
ψ_1	Applied electric potential	Input value
c_b	Bulk ion concentration	Input value

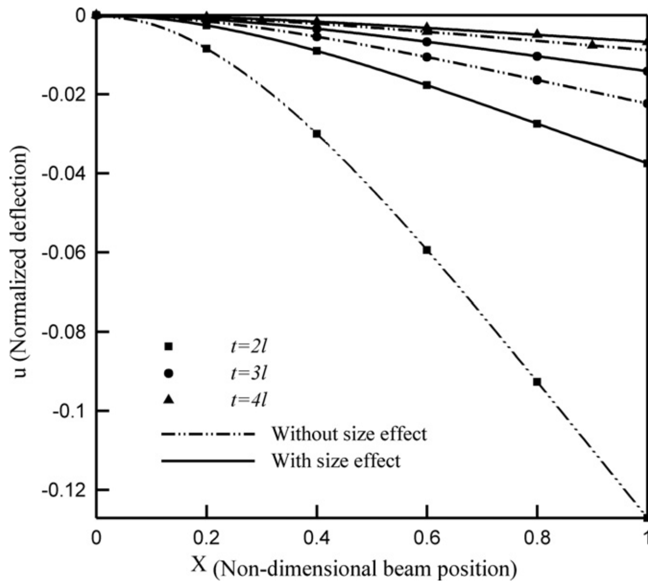

Fig. 9. Effects of beam thickness on deflection for $\psi_1=4$ mV, $c_b=0.05$, $L=200$ μm and $g=1.05$ μm.

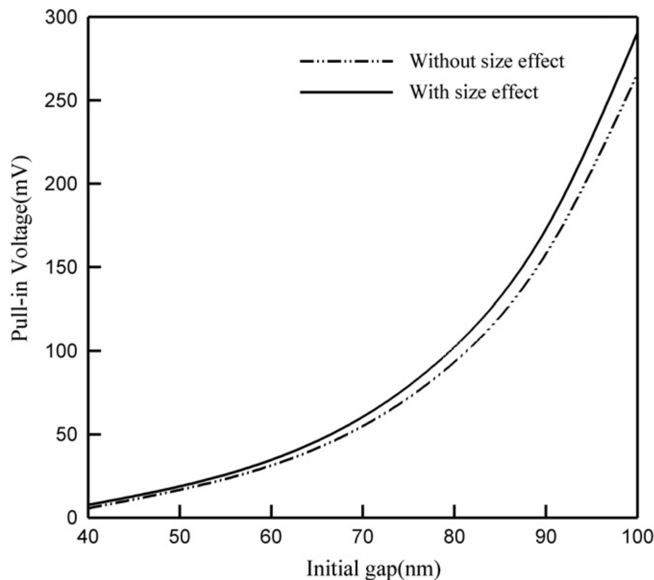

Fig. 10. Effect of initial gap and size dependency on pull-in voltage for $c_b=10^{-3}$, $L=200$ μm and $t=2.94$ μm.

differences between non-classical and classical theory. Therefore, when the thickness of the cantilever is as the order of its length scale parameter, the size effect is significant and the classical beam theory cannot be utilized. Fig. 9 shows that the beam deflection is always smaller by considering size effect than when it is neglected.

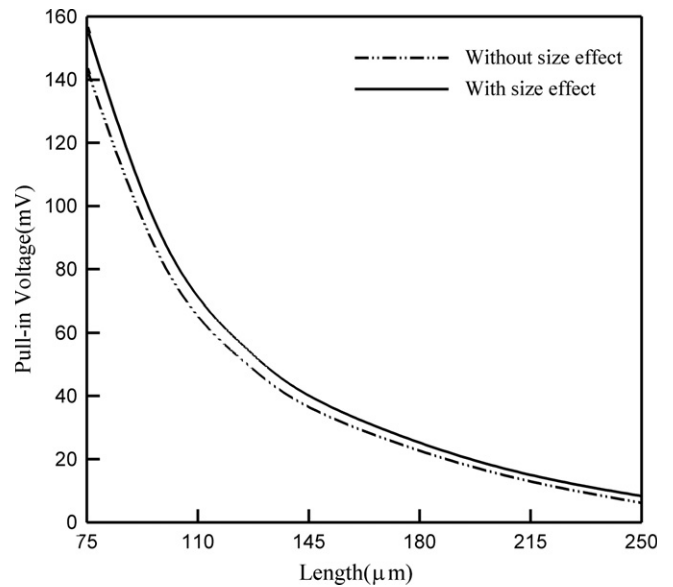

Fig. 11. Effects of length and size dependency on pull-in voltage for $c_b=10^{-3}$, $g=50$ nm and $t=2.94$ μm.

Figs. 10 and 11 indicate the effect of classical and modified couple stress theories on pull-in voltage, $\Delta\psi$, as a function of the initial gap and microactuator length, respectively. Fig. 10 depicts the influence of initial gap and size dependency on the pull-in voltage. As seen, increasing the initial gap increases the pull-in voltage and causes instability in higher voltages. By increasing the initial gap, the influence of size dependency on the pull-in voltage is increased. When the gap decreases, the van der Waals force is increased, and this causes the decreasing of the pull-in voltage. It is concluded that in specifying pull-in voltage of cantilever actuators, the van der Waals force plays a significant role in small gaps.

The effect of microactuator length and size dependency on the pull-in voltage is plotted in Fig. 11. As shown, the pull-in voltage decreases as the length of microactuator increases. This figure reveals that augmentation of the beam length reduces the influence of size effect (modified couple stress theory) on the pull-in voltage.

Figs. 10 and 11 demonstrate that the pull-in voltage is always larger when the size effect is considered. It is concluded that in designing micro/nanobeams actuators, the classical theory predicts the pull-in voltage less than the modified couple stress theory. Thus, the designed micro/nanobeam may fail to switch in practical applications.

Fig. 12 illustrates the effect of ion concentration and size dependency on cantilever tip deflection and pull-in voltage. Augmentation of ion concentration increases the pull-in voltage, but it decreases the magnitude of pull-in deflection. It is seen that increasing ion concentration increases the influence of size dependency on the pull-in voltage. For low ion concentrations, increasing voltage has high influence on the cantilever tip deflection while its influence is reduced as the ion concentration is increased. For a constant ion concentration, size effect causes the increasing of the pull-in voltage, but decreasing the pull-in deflection.

Table 3 shows the dimension and mechanical properties of a practical small scale beam. Fig. 9 depicts the effect of beam thickness on displacement of the beam which identified in

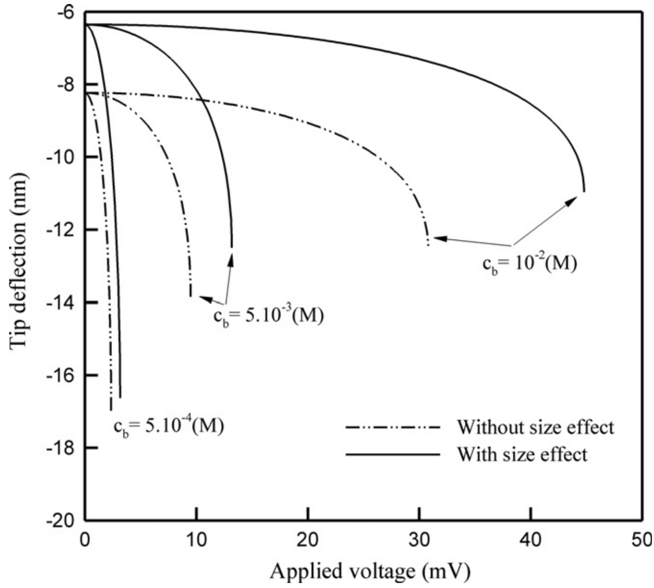

Fig. 12. Effect of ion concentration and size dependency on pull-in parameters and cantilever tip deflection for $L=200$ μm, $g=40$ nm.

Table 3. In order to perform an experimental test, a silicon microbeam switch with the dimension and mechanical properties identified in Table 3 can be constructed. The experimental shape of beam (with different thicknesses) can be compared with the plotted shapes in Fig. 9. The pull-in voltages of the proposed beam also can be compared with the results of Fig. 10 for each different size of gap or Fig. 11 for each different length of beam. Fig. 12 shows tip deflection of beam for different values of bulk ion concentration and applied voltage to cover a range of possible parameters. These figures provide extensive possible case studies which the further practical results can be compared with them.

5. Conclusions

In this research, the influences of size dependency and elastic boundary condition on the static pull-in instability of beam-type micro/nanoactuators immersed in an electrolyte are scrutinized. While the nanobeam is subjected to the van der Waals and electrochemical forces, a non-classical Bernoulli–Euler theory is utilized to consider the size dependency. The obtained nonlinear equation is analytically solved using MAD method. There is good agreement between the analytical and numerical results, even as the micro/nanobeams approach their stability limits. The results show the crucial effects of bulk ion concentration, size dependency and elastic boundary condition on the pull-in parameters of nanobeam. The results can be summarized as follows:

- The electric and van der Waals forces between beam and substrate are always attractive, but the osmotic force is always repulsive. The electrochemical force which is the sum of electric and osmotic forces can be attractive or repulsive depending on the values of the non-dimensional parameters. When the total force (sum of the van der Waals and electrochemical forces) is attractive, the beam bends toward the substrate and pull-in instability may occur. However, when the total force is repulsive, the beam bends upward and there is no pull-in instability.
- Increasing the stiffness parameter decreases the flexibility of the supported end; consequently, less deflection toward the substrate was observed, and more voltage is required to achieve a special deflection.
- Increase of ion concentration increases the pull-in voltage but reduces the pull-in deflection. It is also observed that increasing the ion concentration increases the influence of size-dependent effect on the pull-in voltage.
- Regarding classical theory, the normalized mechanical behaviors of the micro/nanobeam are independent of its dimensions, but by considering the modified couple stress theory, normalized static deflection and pull-in voltage are dependent on the size of micro/nanobeam. Based on modified couple stress theory, the micro/nanobeams are stiffer than those assessed by classical continuum theory.
- Increase of the initial gap increases the magnitude of pull-in voltage as well as the influence of size effect on the pull-in voltage. By contrast, the increase of beam length decreases the magnitude of pull-in voltage as well as the influence of size-dependent effects on pull-in voltage.

Acknowledgements

The authors are grateful to Shahid Chamran University of Ahvaz for its crucial support.

Appendix. Modified Adomian decomposition

Consider a forth-order boundary value problem in the form

$$L^{(4)}[y(x)] = f(x,y\Big),\ 0 \le x \le b \tag{A.1}$$

with boundary conditions

$$y(0) = C_0,\ y'(0) = C_1,\ y''(b) = C_2,\ y'''(b) = C_3 \tag{A.2}$$

where the differential operator $L^{(4)}$ and corresponding inverse operator $L^{-(4)}$ are given by

$$L^{(4)} = \frac{d^{(4)}}{dx^{(4)}} \tag{A.3}$$

$$L^{-(4)} = \int_0^x \int_0^x \int_0^x \int_0^x (.)dx\,dx\,dx\,dx \tag{A.4}$$

The Adomian decomposition method defines the solution $y(x)$ by the decomposition series

$$y(x) = \sum_{n=0}^{\infty} y_n(x) \tag{A.5}$$

and the nonlinear function f(x,y) by an infinite series of polynomials

$$f(x,y) = \sum_{n=0}^{\infty} A_n \tag{A.6}$$

Refer to [64, 65], series A_n can be presented as the following equation

$$A_n = \sum_{v=1}^{n} C(v,n) h_v(y_0) \tag{A.7}$$

where

$$C(v,n) = \sum_{pi} \prod_{i=1}^{v} \frac{y_{pi}^{ki}}{k!},\ \left(\sum_{i=1}^{v} k_i p_i = n, n>0,\ 0 \le i \le n, 1 \le p_i \le n-v+1\right) \tag{A.8}$$

and k_i is the number of repetition in the y_{pi}. Values of p_i are selected from the above range by combination without repetition. $h_v(y_0)$ is calculated by differentiating the nonlinear terms $f(y_0)$, v times with respect to y_0 and can be obtained as

$$h_v(y_0) = \frac{d^v}{dy_0^v}\left[f(y_0)\right] \tag{A.9}$$

Using Eqs.(8–10), the Adomian polynomials can be obtain as

$$\begin{aligned}
A_0 &= h_0(y_0) \\
A_1 &= C(1,1)h_1(y_0) = y_1 h_1(y_0) \\
A_2 &= C(1,2)h_1(y_0) + C(2,2)h_2(y_0) = y_2 h_1(y_0) + \frac{1}{2!}y_1^2 h_2(y_0) \\
A_3 &= C(1,3)h_1(y_0) + C(2,3)h_2(y_0) + C(3,3)h_3(y_0) \\
&= y_3 h_1(y_0) + y_1 y_2 h_2(y_0) + \frac{1}{3!}y_1^3 h_3(y_0) \\
A_4 &= C(1,4)h_1(y_0) + C(2,4)h_2(y_0) + C(3,4)h_3(y_0) + C(4,4)h_4(y_0) \\
&= y_4 h_1(y_0) + h_2(y_0)\left[\frac{1}{2!}y_2^2 + y_1 y_3\right] + \frac{1}{2!}y_1^2 y_2 h_3(y_0) + \frac{1}{4!}y_1^4 h_4(y_0)
\end{aligned} \tag{A.10}$$

Using Adomian decomposition method, the dependent variable in Eq. (1) can be written as

$$y(x) = C_0 + C_1 x + \frac{1}{2!}C_2 x^2 + \frac{1}{3!}C_3 x^3 + L^{-4}\left[\sum_{n=0}^{\infty} A_n\right] \tag{A.11}$$

The boundary conditions at $x=b$ are adequate to evaluate the unknown constants C_2 and C_3 by solving resulted algebraic equation. The recursive relations of Eq. (5) can be provided as

$$\begin{aligned}
y_0 &= C_0 \\
y_1 &= C_1 x + \frac{1}{2!}C_2 x^2 + \frac{1}{3!}C_3 x^3 + L^{-(4)}[A_0] \\
y_{n+1} &= L^{-(4)}[A_n(x)]
\end{aligned} \tag{A.12}$$

Using Eq. (A.10), in Eq. (34) the functions D_n , E_n and F_n are determined through MAD's polynomials as

$$\begin{aligned}
D_0 &= u_0^{-3} \\
D_1 &= -3u_1 u_0^{-4} \\
D_2 &= -3u_2 u_0^{-4} + 6u_1^2 u_0^{-5} \\
D_3 &= -3u_3 u_0^{-4} + 12u_1 u_2 u_0^{-5} - 10u_1^3 u_0^{-6} \\
&\ldots,
\end{aligned} \tag{A.13}$$

$$\begin{aligned}
E_0 &= \cosh(\xi_0 u_0)\sinh(\xi_0 u_0)^{-2} \\
E_1 &= u_1\left(\xi_0 \sinh(\xi_0 u_0)^{-1} - 2\xi_0 \cosh(\xi_0 u_0)^2 \sinh(\xi_0 u_0)^{-3}\right) \\
E_2 &= u_2\left(\xi_0 \sinh(\xi_0 u_0)^{-1} - 2\xi_0 \cosh(\xi_0 u_0)^2 \sinh(\xi_0 u_0)^{-3}\right) \\
&\quad + \frac{1}{2}u_1^2\left(-5\xi_0^2 \cosh(\xi_0 u_0)\sinh(\xi_0 u_0)^{-2} + 6\xi_0^2 \cosh(\xi_0 u_0)^3 \sinh(\xi_0 u_0)^{-4}\right) \\
E_3 &= u_3\left(\xi_0 \sinh(\xi_0 u_0)^{-1} - 2\xi_0 \cosh(\xi_0 u_0)^2 \sinh(\xi_0 u_0)^{-3}\right) \\
&\quad + u_1 u_2\left(-5\xi_0^2 \cosh(\xi_0 u_0)\sinh(\xi_0 u_0)^{-2} + 6\xi_0^2 \cosh(\xi_0 u_0)^3 \sinh(\xi_0 u_0)^{-4}\right) \\
&\quad + \frac{1}{6}u_1^3\left(28\xi_0^3 \cosh(\xi_0 u_0)^2 \sinh(\xi_0 u_0)^{-3} - 5\xi_0^3 \sinh(\xi_0 u_0)^{-1}\right. \\
&\quad \left. - 24\xi_0^3 \cosh(\xi_0 u_0)^4 \sinh(\xi_0 u_0)^{-5}\right) \\
&\ldots,
\end{aligned} \tag{A.14}$$

and

$$\begin{aligned}
F_0 &= \sinh(\xi_0 u_0)^{-2} \\
F_1 &= -2u_1 \xi_0 \cosh(\xi_0 u_0)\sinh(\xi_0 u_0)^{-3} \\
F_2 &= -2u_2 \xi_0 \cosh(\xi_0 u_0)\sinh(\xi_0 u_0)^{-3} \\
&\quad + \frac{1}{2}u_1^2\left(6\xi_0^2 \cosh(\xi_0 u_0)^2 \sinh(\xi_0 u_0)^{-4} - 2\xi_0^2 \sinh(\xi_0 u_0)^{-2}\right) \\
F_3 &= -2u_3 \xi_0 \cosh(\xi_0 u_0)\sinh(\xi_0 u_0)^{-3} \\
&\quad + u_1 u_2\left(6\xi_0^2 \cosh(\xi_0 u_0)^2 \sinh(\xi_0 u_0)^{-4} - 2\xi_0^2 \sinh(\xi_0 u_0)^{-2}\right) \\
&\quad + \frac{1}{6}u_1^3\left(-24\xi_0^3 \cosh(\xi_0 u_0)^3 \sinh(\xi_0 u_0)^{-5}\right. \\
&\quad \left. + 16\xi_0^3 \cosh(\xi_0 u_0)\sinh(\xi_0 u_0)^{-3}\right) \\
&\ldots,
\end{aligned} \tag{A.15}$$

By substituting relations (A.13)–(A.15) in Eq. (33) the components u_n(x) can be determined as follow

$$\begin{aligned}
u_0 &= 1 \\
u_1 &= C_1 X + \frac{1}{2!}C_2 X^2 + \frac{1}{3!}C_3 X^3 - \frac{1}{4!}\frac{1}{(1+\delta)}X^4\left(\alpha - \beta\frac{\phi_2}{\phi_1}\frac{\cosh(\xi_0)}{\sinh(\xi_0)^2} + \beta\left(1 + \left(\frac{\phi_2}{\phi_1}\right)^2\right)\frac{1}{2\sinh(\xi_0)^2}\right) \\
u_2 &= \frac{1}{(1+\delta)}\left(3\alpha + \beta\frac{\phi_2}{\phi_1}\frac{\xi_0}{\sinh(\xi_0)}\left(1 - \frac{2\cosh(\xi_0)^2}{\sinh(\xi_0)^2}\right) + \beta\left(1 + \left(\frac{\phi_2}{\phi_1}\right)^2\right)\frac{\xi_0 \cosh(\xi_0)}{\sinh(\xi_0)^3}\right) \\
&\quad \times\left(\frac{C_1}{5!}X^5 + \frac{C_2}{6!}X^6 + \frac{C_3}{7!}X^7 + \frac{1}{8!}\frac{1}{(1+\delta)}X^8\left(-\alpha + \beta\frac{\phi_2}{\phi_1}\frac{\cosh(\xi_0)}{\sinh(\xi_0)^2} - \beta\left(1 + \left(\frac{\phi_2}{\phi_1}\right)^2\right)\frac{1}{2\sinh(\xi_0)^2}\right)\right)
\end{aligned} \tag{A.16}$$

References

[1] K.H.L. Chau, S.R. Lewis, Y. Zhao, R.T. Howe, S.F. Bart, R.G. Marcheselli, An Integrated force-balanced capacitive accelerometer for low-*g* applications, Sensors and Actuators A: Physical 54 (1996) 472–476.

[2] C. Lu, M. Lemkin, B.E. Boser, A monolithic surface micro machined accelerometer with digital output, IEEE Journal of Solid-State Circuits 30 (1995) 1367–1373.

[3] L. Parameswaran, A. Mirza, W.K. Chan, M.A. Schmidt, Silicon pressure sensors using a wafer-bonded sealed cavity process, in: Proceedings of Transducers; 95 Eurosensors IX Solid-State Sensors and Actuators, Stockholm, Sweden, 1995, pp. 582–585.

[4] K. Wang, C.T.C. Nguyen, High-order micromechanical electronic filters, in: Proceedings of IEEE Micro Electro Mechanical Systems, Nagoyo, Japan, 1997, pp. 25–30.

[5] W.P. Taylor, M.G. Allen, C.R. Dauwalter, Fully integrated magnetically actuated micro machined relays, Journal of Microelectromechanical Systems 7 (1998) 181–191.

[6] P. Kim, C.M. Lieber, Nanotube nanotweezers, Science 286 (1999) 2148–2150.

[7] S. Akita, Y. Nakayama, S. Mizooka, Y. Takano, Nanotweezers consisting of carbon nanotubes operating in an atomic force microscope, Applied Physics Letters 79 (2001) 1691–1693.

[8] G.M. Rebeiz, J.B. Muldavin, RF MEMS switches and switch circuits, IEEE Microwave Magazine 2 (2001) 59–71.

[9] V. Mukundan, B.L. Pruitt, MEMS electrostatic actuation in conducting biological media, Journal of Microelectromechanical Systems 18 (2009) 405–413.

[10] M. Ghalambaz, A. Noghrehabadi, M. Abadyan, Y.T. Beni, A.N. Abadi, M.N. Abadi, A new power series solution on the electrostatic pull-in instability of nano cantilever actuators, Procedia Engineering 10 (2011) 3708–3716.

[11] A. Soroush, A. Koochi, A.S. Kazemi, A. Noghrehabadi, H. Haddadpour, M. Abadyan, Investigating the effect of Casimir and van der Waals attractions on the electrostatic pull-in instability of nano-actuators, Physica Scripta 82 (2010) 045801-045801.

[12] C.H. Mastrangelo, C.H. Hsu, Mechanical stability and adhesion of microstructures under capillary force-Part I: Basic theory, Journal of Microelectromechanical Systems 2 (1993) 33–43.

[13] J.N. Israelachvili, Intermolecular and Surface Forces, Academic Press, London, 1992.

[14] P.M. Osterberg, Electrostatically Actuated micro Electromechanical Test Structures for Material Property Measurements, in: Ph.D. Dissertation, Massachusette Institute of Technology (MIT), Cambridge, 1995.

[15] W.H. Lin, Y.P. Zhao, Pull-in Instability of micro-switch actuators: model review, International Journal of Nonlinear Sciences and Numerical Simulation 9 (2008) 175–183.

[16] O. Bochobza-Degani, E. Socher, Y. Nemirovsky, On the effect of residual charges on the pull-in parameters of electrostatic actuators, Journal of Sensors and Actuators A 97–98 (2002) 563–568.

[17] O. Degani, Y. Nemirovsky, Design donsiderations of rectangular electrostatic torsion actuators based on new analytical pull-in expressions, Journal of Microelectromechanical Systems 11 (2002) 20–26.

[18] S. Chowdhury, M. Ahmadi, W.C. Miller, A closed-form model for the pull-in voltage of electrostatically actuated cantilever beams, Journal of Micromechanics and Microengineering 15 (2005) 756–763.

[19] F.M. Serry, D. Walliser, G.J. Maclay, The role of the Casimir effect in the static deflection and stiction of membrane strips in micro electromechanical systems (MEMS), Journal of Applied Physics 84 (1998) 2501–2506.

[20] W.H. Lin, Y.P. Zhao, Nonlinear behavior for nanoscale electrostatic actuators with Casimir force, Chaos, Solitons & Fractals 23 (2005) 1777–1785.

[21] W.H. Lin, Y.P. Zhao, Casimir effect on the pull-in parameters of nanometer switches, Microsystem Technologies 11 (2005) 80–85.

[22] K.S. Ou, K.S. Chen, T.S. Yang, S.Y. Lee, A novel semianalytical approach for finding pull-in voltages of micro cantilever beams subjected to electrostatic loads and residual stress gradients, Journal of Microelectromechanical Systems 20 (2011) 527–537.
[23] A. Noghrehabad, M. Ghalambaz, A. Ghanbarzadeh, A new approach to the electrostatic pull-in instability of nanocantilever actuators using the ADM-Padé technique, Computers & Mathematics with Applications 64 (2012) 2806–2815.
[24] A. Noghrehabadi, Y.T. Beni, A. Koochi, A. Kazemi, A. Yekrangi, M. Abadyan, M.N. Abadi, Closed-form approximations of the pull-in parameters and stress field of electrostatic cantilevers nano-actuators considering van der Waals attraction, Procedia Engineering 10 (2011) 3750–3756.
[25] A. Ramezani, A. Alasty, J. Akbari, Analytical investigation and numerical verification of Casimir effect on electrostatic nano-cantilever, Microsystem Technologies 14 (2007) 145–157.
[26] A. Ramezani, A. Alasty, J. Akbari, Closed-form solutions of the pull-in instability in nano-cantilevers under electrostatic and intermolecular surface forces, International Journal of Solids and Structures 44 (2007) 4925–4941.
[27] M.R. Abadyan, Y.T. Beni, A. Noghrehabadi, Investigation of elastic boundary condition on the pull-in instability of beam-type NEMS under van der Waals attraction, Procedia Engineering 10 (2011) 1724–1729.
[28] A. Noghrehabadi, M. Ghalambaz, Y.T. Beni, M. Abadyan, M.N. Abadi, M.N. Abadi, A new solution on the buckling and stable length of multi wall carbon nanotube probes near graphite sheets, Procedia Engineering 10 (2011) 3725–3733.
[29] A. Noghrehabadi, M. Ghalambaz, A. Ghanbarzadeh, Buckling of multi wall carbon nanotube cantilevers in the vicinity of graphite sheets using monotone positive method, Journal of Computational and Applied Research in Mechanical Engineering 1 (2012) 89–97.
[30] J.G. Guo, Y.P. Zhao, Influence of van der Waals and Casimir forces on electrostatic torsional actuators, Journal of Microelectromechanical Systems 13 (2004) 1027–1035.
[31] A. Gusso, G.J. Delben, Influence of the Casimir force on the pull-in parameters of silicon based electrostatic torsional actuators, Sensors and Actuators A: Physical 135 (2007) 792–800.
[32] J.S. Stolken, A.G. Evans, Microbend test method for measuring the plasticity length scale, Acta Materialia 46 (1998) 5109–5115.
[33] W.D. Nix, H. Gao, Indentation size effects in crystalline materials: a law for strain gradient plasticity, Journal of the Mechanics and Physics of Solids 46 (1998) 411–425.
[34] K.W. McElhaney, J.J. Vlassak, W.D. Nix, Determination of indenter tip geometry and indentation contact area for depth-sensing indentation experiments, Journal of Materials Research 13 (1998) 1300–1306.
[35] S.K. Park, X.L. Gao, Bernoulli–Euler beam model based on a modified couple stress theory, Journal of Micromechanics and Microengineering 16 (2006) 2355–2359.
[36] M. Rahaeifard, M.H. Kahrobaiyan, M.T. Ahmadian, K. Firoozbakhsh, Size-dependent pull-in phenomena in nonlinear microbridges, International Journal of Mechanical Sciences 54 (2012) 306–310.
[37] B. Akgöz, Ö. Civalek, Strain gradient elasticity and modified couple stress models for buckling analysis of axially loaded micro-scaled beams, International Journal of Engineering Science 49 (2011) 1268–1280.
[38] F. Yang, A.C.M. Chong, D.C.C. Lam, P. Tong, Couple stress based strain gradient theory for elasticity, International Journal of Solids and Structures 39 (2002) 2731–2743.
[39] S. Kong, S. Zhou, Z. Nie, K. Wang, The size-dependent natural frequency of Bernoulli–Euler micro-beams, International Journal of Engineering Science 46 (2008) 427–437.
[40] J. Zhao, S. Zhou, B. Wang, Size dependent pull-in phenomena in electrostatically actuated micro-beam based on the modified couple stress theory, Advances in Materials Research 335–336 (2011) 633–640.
[41] Y.T. Beni, M.R. Abadyan, A. Noghrehabadi, Investigation of size effect on the pull-in instability of beamtype NEMS under van der Waals attraction, Procedia Engineering 10 (2011) 1718–1723.
[42] H. Sadeghian, C.K. Yang, J.F.L. Goosen, A. Bossche, U. Staufer, P.J. French, F.V. Keulen, Effects of size and defects on the elasticity of silicon nanocantilevers, Journal of Micromechanics and Microengineering 20 (2010) 1–8.
[43] G. Rinaldi, M. Packirisamy, I. Stiharu, Multiparameter synthesis of microsystems, in: Proceedings of SPIE, International Conference on Photonic Devices, 2005, pp. 333–344.
[44] R.L. Mullen, M. Mehregany, M. Omar, W.H. Ko, Theoretical modeling of boundary conditions in microfabricated beams, in: Proceedings of IEEE Micro Electro Mechanical Systems, Nara, Japan, 1991, pp. 154–159.
[45] G. Rinaldi, M. Packirisamy, I. Stiharu, Experimental investigation on the dynamics of MEMS structures, in: Proceedings of SPIE Photonics Europe: MEMS, MOEMS and Micromachining, Strasbourg, France, 2004, pp. 66–73.
[46] L. Yunqiang, P. Muthukumaran, B.B. Rama, Shape optimizations and static/dynamic characterizations of deformable microplate structures with multiple electrostatic actuators, Microsystem Technologies 14 (2008) 255–266.
[47] G. Rinaldi, M. Packirisamy, I. Stiharu, Quantitative boundary support characterization for cantilever MEMS, Sensors 7 (2007) 2062–2079.
[48] T.L. Sounart, T.A. Michalske, K.R. Zavadil, Frequency-dependent electrostatic actuation in microfluidic MEMS, Journal of Microelectromechanical Systems 14 (2005) 125–133.
[49] J.G. Boyd, D. Kim, Nanoscale electrostatic actuators in liquid electrolytes, Journal of Colloid and Interface Science 301 (2006) 542–548.
[50] J.G. Boyd, J. Lee, Deflection and pull-in instability of nanoscale beams in liquid electrolytes, Journal of Colloid and Interface Science 356 (2011) 387–394.
[51] E. Jomehzadeh, H.R. Noori, A.R. Saidi, The size-dependent vibration analysis of micro-plates based on a modifiedcouple stress theory, Physica E: Low-dimensional Systems and Nanostructures 43 (2011) 877–883.
[52] R.D. Mindlin, Influence of couple-stresses on stress concentrations, Experimental Mechanics 3 (1963) 1–7.
[53] C.H. Ke, H.D. Espinosa, N. Pugno, Numerical analysis of nanotube based NEMS devices-part II: Role of finite kinematics, stretching and charge concentrations, Journal of Applied Mechanics 72 (2005) 726–731.
[54] D. Kim, Nanosclae Electrostatic Actuators in Liquid Electrolytes: Analysis and Experiment, Ph.D. Dissertation, A&M, TX, 2008.
[55] W.H. Lin, Y.P. Zhao, Dynamic behaviour of nanoscale electrostatic actuators, Chinese Physics Letters 20 (2003) 2070–2073.
[56] M. Rahaeifard, M.H. Kahrobaiyan, M. Asghari, M.T. Ahmadian, Static pull-in analysis of microcantilevers based on the modified couple stress theory, Sensors and Actuators A: Physical 171 (2011) 370–374.
[57] W.H. Lin, Y.P. Zhao, Influence of damping on the dynamical behavior of the electrostatic parallel-plate and torsional actuators with intermolecular forces, Sensors 7 (2007) 3012–3026.
[58] D. Andelman, Electrostatic properties of membranes: the Poisson–Boltzmann theory, Handbook of Biological Physics 1 (1995) 603–642.
[59] A.M. Wazwaz, The numerical solution of sixth-order boundary value problems by the modified decomposition method, Applied Mathematics and Computation 118 (2001) 311–325.
[60] R. Rach, A convenient computational form for the Adomian polynomials, Journal of Mathematical Analysis and Applications 102 (1984) 415–419.
[61] G. Adomian, Nonlinear Stochastic Operator Equations, Landon, Academic press, 1986.
[62] E.H. Aly, A. Ebaid, R. Rach, Advances in the Adomian decomposition method for solving two-point nonlinear boundary value problems with Neumann boundary conditions, Computers & Mathematics with Applications 63 (2012) 1056–1065.
[63] J.S. Duan, T. Chaolu, R. Rach, Solutions of the initial value problem for nonlinear fractional ordinary differential equations by the Rach–Adomian–Meyers modified decomposition method, Applied Mathematics and Computation 218 (2012) 8370–8392.
[64] J.S. Duan, R. Rach, New higher-order numerical one-step methods based on the Adomian and the modified decomposition methods, Applied Mathematics and Computation 218 (2011) 2810–2828.
[65] J.S. Duan, R. Rach, Higher-order numeric Wazwaz-El-Sayed modified Adomian decomposition algorithms, Computers & Mathematics with Applications 63 (2012) 1557–1568.
[66] R. Rach, J.S. Duan, Near-field and far-field approximations by the Adomian and asymptotic decomposition methods, Applied Mathematics and Computation 217 (2011) 5910–5922.